Experimental study on compressive behavior and failure analysis of composite concrete confined by glass/epoxy ±55° filament wound pipes

Lokman Gemi[a], Mehmet Alpaslan Köroğlu[b*], Ashraf Ashour[c]

[a] *Meram Vocational School, Necmettin Erbakan University, Dere Aşıklar Mah. Demeç Sok. No:42/A 42140 Meram, Konya, Turkey.*

[b] *Civil Engineering Department, Faculty of Engineering and Architecture, Necmettin Erbakan University, Dere Aşıklar Mah. Demeç Sok. No:42/A 42140 Meram, Konya, Turkey. (*Corresponding Author makoroglu@konya.edu.tr)*

[c] *Faculty of Engineering & Informatics, University of Bradford, Bradford, West Yorkshire, BD7 1DP, UK*

ABSTRACT

This paper investigates the strength and ductility of concrete confined by Glass/Epoxy ±55° Filament Wound Pipes (GFRP) under axial compression. A total of 24 cylinderical specimens were prepared with expansive and Portland cements, properly compacted and un-compacted for different composite fresh concrete matrix. Test results showed that compressive strength and axial deformation at failure of concrete confined with GFRP tubes increased by an average of 2.85 and 5.57 times these of unconfined concrete, respectively. Macro and micro analyses of GFRP pipes after failure were also investigated. Debonding, whitening, matrix/transfer cracking, delamination and splitting mechanisms were detected at failure, respectively. The experimental results were also employed to assess the reliability of design models available in the literature for confined concrete compressive strength.

Keywords: GFRP tubes, Composite column, Uniaxial strength, Filament winding, Damage mechanism, Confined concrete, Fiber orientation, Debonding, Micro structure.

1. Introduction

Corrosion of steel reinforcement due to harsh environment is a major cause of deterioration of performance of reinforced concrete columns. Various strengthening techniques have been developed to restore the column capacity and ductility, for example wrapping reinforced concrete columns by fibre reinforced polymer (FRP) jackets. However, in the last two decades, concrete filled FRP tube columns have been proposed as an alternative technique for protecting the internal steel reinforcement against corrosion. In fact, FRP tubes not only preserve steel reinforcement from corrosion but also act as confining reinforcement in the transverse direction.

For strengthening concrete members, external confinement with FRP jackets has become a common practice in construction industry. A significant number of experimental studies on compressive behaviour of FRP-confined concrete have been carried out over the past two decades. However, studies focused on FRP tubes are still limited [1-9]. Nevertheless, the high inelastic deformational capacity of concrete confined with FRP tubes has been a remarkable alternative for innovative high-performance columns [10].

A great number of investigations have focused on hoop direction of specimens wrapped with FRP sheets. 24 concrete filled FRP tubes (CFFT) with 15 degrees aligned glass fibres specimens were tested by Mirmiran and Shahawy in order to explore the influence of FRP thickness [11]. Similarly, La Tegola and Manni [12] experimented 10 different CFFTs with filaments aligned at 55 and 77 degrees. Rochette and Labossiere [13] studied CFFT specimens with fibres aligned at 15 degrees. Pessiki et al. [14] tested CFFT specimens with fibre alignment of 0 and 45 degrees. Not only cylindrical concrete specimens but also full scale test specimens wrapped with FRP sheets were tested by many researchers. Studies on orientation of confining fibres and fibre angles that are the essential parameters on the behaviour of compressive strength of FRP-confined concrete were analysed [15-18]. Vincent and Ozbakkaloglu [19] investigated the effect of fibre alignment with angles 45, 60, 75 and 88 degrees on the axial load capacity of FRP-confined concrete and concluded that both axial strength and strain enhancement ratios substantially increased as the fibre orientation increases with respect to the longitudinal axis. However, in the current investigation, ±55° winding angle is selected for the purpose of columns required to resist the combined effect of both axial and lateral loadings as recommended in another study [20].

On-site concrete production is generally consolidated with internal vibrator, which is an operator-sensitive process, especially in concrete deep piles where visibility and accessibility are restricted and, therefore, proper concrete consolidation is exclusively difficult to achieve. On the other hand, segregation of concrete core due to over-consolidation may occur. Additionally, voids and cavities in under-consolidated concrete not only lead to air contained in concrete that may cause steel reinforcement corrosion but also decrease concrete compressive strength. In order to alleviate the problem of corrosion, fresh concrete can be poured into FRP tubes, acting as protective jacket in aggressive environments as well as structural formwork.

Fibre-reinforced polymer (FRP) composites have been widely used as internal and external reinforcements to concrete structures, for example as reinforcement in beams or slabs [21-23]. Nowadays, composite FRP piles have been an innovative solution for composite columns. There are a great number of experimental and analytical studies in the literature focusing on hoop stress behavior of glass–epoxy composites pipes [20, 24-30]. Macro and micro analyses of the damage progression of composite piles without concrete under impact loading and internal pressure (hoop) have been widely carried out in the literature [28, 31, 32]. However, macro and micro damage mechanisms of the composite pipes with concrete under hoop direction loadings have not been thoroughly investigated in the literature.

The aim of this experimental study is to investigate the confinement effect of Glass/Epoxy $\pm 55^{\circ}$ filament wound pipes on the axial load capacity and ductility of short cylindrical pipes filled with different types of concrete subjected to uniaxial compression. Specimens produced with Portland and expansive cements were studied to examine the effect of interfacial contact between concrete and confined pipes. On account of examining the consolidation of fresh concrete, half of the specimens were casted without fresh concrete vibration. Micro and macro analyses of selected GFRP pipes after failure were investigated.

2. Materials and Methods

A total of 24 cylindrical specimens having the same dimensions of 72x160mm were constructed and tested under uniaxial compression. The main parameters investigated were the cement type used, water/cement ratio,

confinement by glass filament wound pipes and vibration of fresh concrete. Table 1 lists all test specimens and parameters considered. Two different cement types were used in concrete mixture, namely Portland cement (PC) in 12 specimens and expansive cement (EC) in the other 12 specimens. Water/cement ratios considered were 0.4, 0.5 and 0.6. 12 specimens were confined with glass filament wound pipes and the other 12 were tested un-confinement. Furthermore, twelve of the tested specimens were compacted during the concrete casting process whereas the other twelve were not compacted.

Each test specimen is identified by three or four letters as explained below. “PC” is used for the specimens produced with Portland cement whereas “EC” is used for the specimens produced with expansive cement. The second number identifies the w/c cement ratio of 0.6, 0.5 or 0.4. Furthermore, the third character “C” or “NC” refers to the compacted fresh concrete or uncompacted specimens, respectively. The last character “T” is used only for specimens confined with GFRP pipes.

2.1. Concrete

Six concrete mixtures projected to accomplish different 28-day cylinder compressive strengths were used for casting the concrete specimens. The ingredient proportions of cement, aggregate, sand, water and admixture proportions and the 28 days compressive strength of each mixture are shown in Table 1. CEM I 32.5 R type cement was used to prepare the normal composite concrete (NCC) mixture whereas the other mixture was prepared using expansive cement (EC) instead of CEM I 32.5 R. For all specimens, nylon polymers (20 kg/m3; 0,83% by weight) were used in order to control shrinkage cracks and minimize settlement shrinkage. The nylon polymers used was 100% virgin nylon fibrous monofilament, having 19 mm length and 966 MPa tensile strength. For each concrete batch, 3 cubes with dimensions of 100*100*100 mm were prepared and tested after 28 days. The average compressive strength of concrete cubes for each specimen is given in Table 1.

Table 1. Concrete mixture elements and their obtained mechanical properties

Specimen	w/c ratio	Water (kg/m3)	Cement (kg/m3)	Aggregate (kg/m3)	Nylon Polymer (kg/m3)	Cement type	Vibration used	GFRP Tube	Compressive strength of concrete at 28 days (MPa)
PC-0,6-C- T	0,6	132	219	2049	20	Portland	✓	✓	17
PC-0,5-C-T	0,5	160	320	1920	20	Portland	✓	✓	22
PC-0,4-C-T	0,4	158	392	1850	20	Portland	✓	✓	23
EC-0,6-C-T	0,6	132	219	2160	20	expansive	✓	✓	27
EC-0,5-C-T	0,5	160	320	1920	20	expansive	✓	✓	32
EC-0,4-C-T	0,4	158	392	1720	20	expansive	✓	✓	38
PC-0,6-NC-T	0,6	132	219	2049	20	expansive	-	✓	15
PC-0,5-NC-T	0,5	160	320	1920	20	Portland	-	✓	20

PC-0,4-NC-T	0,4	158	392	1850	20	Portland	-	✓	22
EC-0,6-NC-T	0,6	132	219	2160	20	expansive	-	✓	25
EC-0,5-NC-T	0,5	160	320	1920	20	expansive	-	✓	29
EC-0,4-NC-T	0,4	158	392	1720	20	expansive	-	✓	35
PC-0,6-C	0,6	132	219	2049	20	Portland	✓	-	17
PC-0,5-C	0,5	160	320	1920	20	Portland	✓	-	22
PC-0,4-C	0,4	158	392	1850	20	Portland	✓	-	23
EC-0,6-C	0,6	132	219	2160	20	expansive	✓	-	27
EC-0,5-C	0,5	160	320	1920	20	expansive	✓	-	32
EC-0,4-C	0,4	158	392	1720	20	expansive	✓	-	38
PC-0,6-NC	0,6	132	219	2049	20	Portland	-	-	15
PC-0,5-NC	0,5	160	320	1920	20	Portland	-	-	20
PC-0,4-NC	0,4	158	392	1850	20	Portland	-	-	22
EC-0,6-NC	0,6	132	219	2160	20	expansive	-	-	25
EC-0,5-NC	0,5	160	320	1920	20	expansive	-	-	29
EC-0,4-NC	0,4	158	392	1720	20	expansive	-	-	35

2.2. GFRP tubes manufacturing and mechanical properties

The GFRP composite tubes used in this study were produced with three layers of fibres using filament winding technique in such a way that the winding angle is $\pm 55^{\circ}$ as shown in Fig. 1. The fibre material used in the tubes was Vetrotex 1200 tex E-glass with 17µm diameters whereas the matrix was Bisophenol A, Epoxy CY 225. After being manufactured, the $(\pm 55^{\circ})_3$ tubes were, initially, cured in an oven at a temperature of 135°C for two hours and, then, cured at 150°C temperature for another two hours. The length, inner diameter, and thickness of the tubes were 160 mm, 72 mm, and 2.4 ± 0.04 mm, respectively (Fig. 2(a)). The properties of the fibres and matrix used are given in Table 2, while the mechanical properties of the GFRP tubes are shown in Table 3. The mechanical properties of GFRP tubes are calculated from hydraulic burst pressure test (See Fig. 2(b)) according to ASTM D1599 (2005) standards [33]. The tangential failure stress, strain ratio and elastic modulus were calculated from the measured inner pressure, horizontal and vertical strains at failure from burst pressure test.

Fig. 1. Filament winding technique

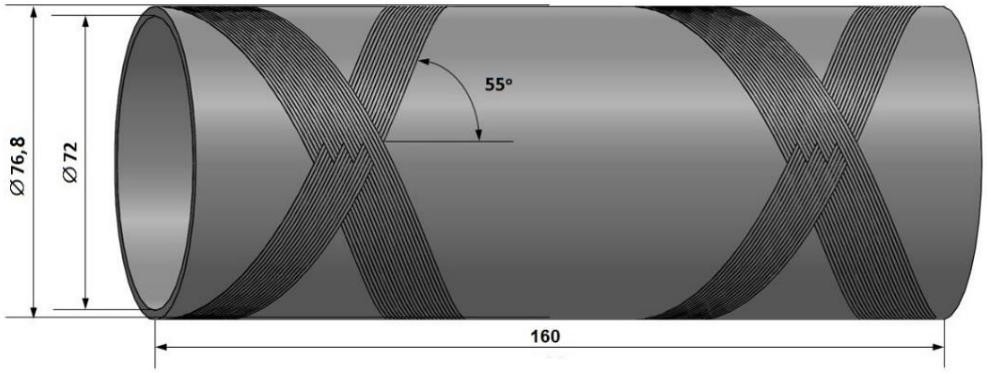

(a) Geometrical dimensions of GFRP tubes

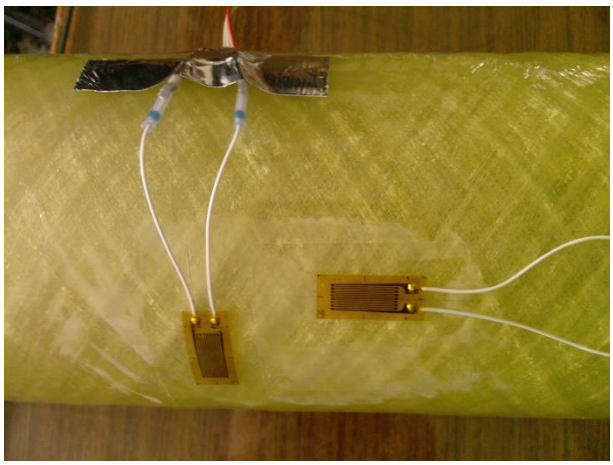

(b) Hydraulic burst pressure test

Fig. 2. Geometrical dimensions and hydraulic burst pressure test of tubes used

Table 2. Properties of fibres and resin.

	Elasticity Modulus (GPa)	Tensile Strength (MPa)	Density (g/cm^3)	Strain at Fracture (%)
Fibre: E-glass	73.10	2345	2.60	1.50-2.00
Matrix: Epoxy resin	3.40	50-60	1.20	4.00-6.00

Table 3. Properties of composite tubes used.

θ	Winding angle (Glass)	$\pm 55^{\circ}$
σ_T	Tangential failure stress (MPa)	429
ν_y	Strain ratio ($\varepsilon_T/\ \varepsilon_{HS}$)	0.53
E_y	Elastic modulus in tangential direction (GPa)	20.48
V_f	Fibres volume fraction	0.50

According to ASTM D 2584, the fibre volume fraction values of the samples are determined by the following equation Vf = $(W_f/\rho_f)/(W_c/\rho_c)$, where W_f is the mass of fibre, W_c is the weight of composite pipe, ρ_f is the density of fibre and ρ_c is the density of composite pipe.

3. Experimental Study

Composite concrete and concrete-filled GFRP tube composite cylinders were produced in accordance to TS EN 206 [34]. However, for twelve specimens, rodding or vibration was not carried out to examine the effect of consolidation of fresh concrete on compressive strength of hardened concrete. All concrete mixtures were produced in the laboratory by rotary concrete mixer and all specimens were cured in a curing tank for 27 days. Compressive strength of all hardened concrete cylindrical specimens utilized for the uniaxial compression test is given in Table 1.

For each cylinder, axial shortening was measured by two linear variable displacement transducers (LVDTs) located 180 degrees apart along the hoop direction of the test specimen. A circular steel plate of 5 mm thickness and 70 mm diameter is plastered on both top and bottom surfaces of concrete in order to transfer the load uniformly to the whole cross-section of the cylindrical specimens. 2 mm gap is applied between steel plates and concrete on account of preventing the contact between the tube and head of test machine when the load is applied as shown in Fig. 3a. All GFRP tube composite cylinders were tested under axial compression using a 500-kN capacity compression testing machine at a loading rate of 4.5 kN/s by automatic controlled hydraulic pump. The tubes were setup vertically at the center of the loading plates of the machine during the tests (Fig. 3).

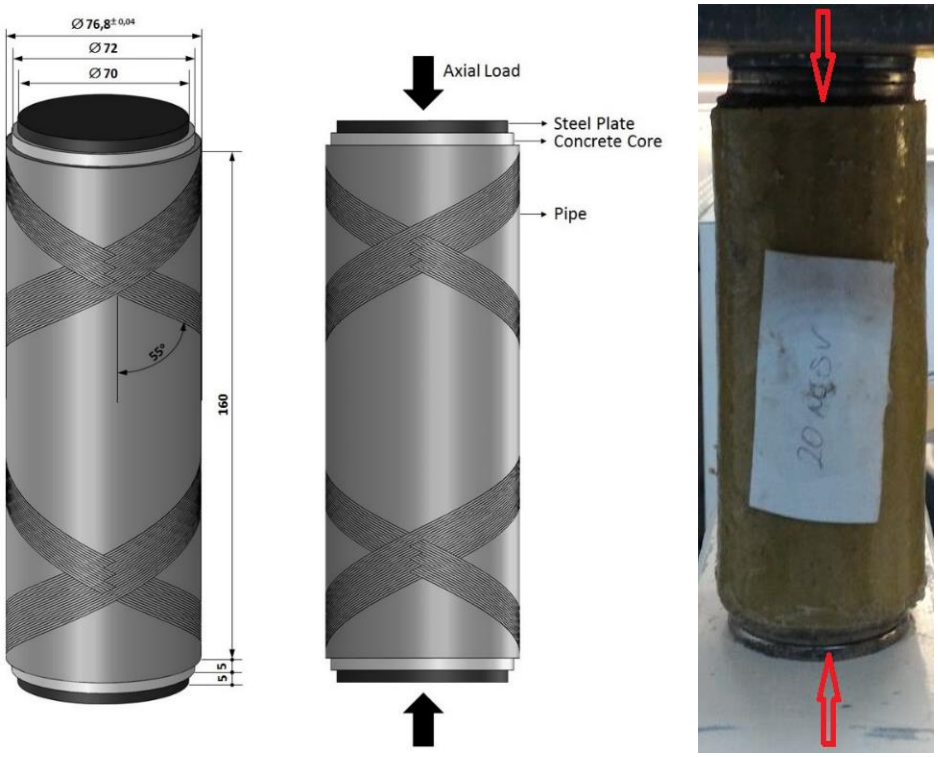

Fig. 3. a) Composite concrete-filled GFRP tube b) GFRP tube composite cylinders tested under axial compression

3.1. Results and discussion of compression tests

Fig. 4 shows the axial load-axial deformation relationships for typical three specimens, namely very low, low and high concrete compressive strength. It is observed that the trend can be categorised by three different regions as observed in other investigations [35, 36] and explained below. The first region is characterised by the initial linear elastic behaviour [35, 36], whereas the third region is signified by the linear, strain hardening part before failure. On the other hand, the non-linear trend between the two linear regions identifies the middle transition second region. For the initial linear region, concrete behaviour is dominant whereas GFRP tube characteristic is dominant for the third linear region. However, the second region is nonlinear stage owing to the intensive cracks on concrete under confinement effect. In the first region of the loading process, all confined specimens behaved in a similar way. At about 40% of the ultimate load, loud sound signifying concrete cracking was clear, demonstrating the non-linear behaviour of the load-deformation of the second region. Due to the stress increase in fibres, white marks were detected at about 60% of the ultimate load. In the second nonlinear region, the effect of the tube confinement is activated due to the increase of lateral strains and occurrence of micro-cracks as observed in other investigation [35]. At this stage, whitening of FRP tube has developed throughout the filaments at $\pm 55^{\circ}$ according to the longitudinal axis. As the load increased, the white coloured area on the tube has developed on the second stage. As seen in Fig. 4, the effect of compressive strength of concrete dominated the behaviour of the second stage. For example, the presence of voids in concrete strength extended the transition region. Therefore, uncompacted specimens which have low concrete compression

strength have long second stage. At the end of the last stage, a sudden rupture of the fibres occurred, leading to the specimen failure.

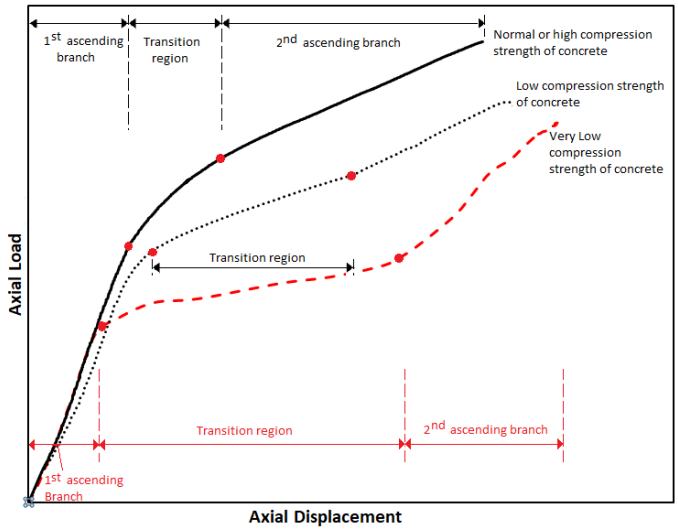

Fig. 4. Illustration of different stages of axial load–displacement curves

Although specimens with various concrete compressive strength, which are indirectly affected by the compaction of concrete, have different second region behaviour, they generally exhibited similar failure characteristics. In general, the axial load capacity of tubes improved by nearly 3.5 times compared to unconfined concrete cylindrical specimens due to the confinement effect of GFRP.

For uncompacted specimens due to the voids created in concrete, failure development maintained longer axial displacement during the second region. Subsequently, white lines demonstrating the development of streeses in the fibres initiated to advance throughout the fibres at $\pm 55^{\circ}$ in accordance with the longitudinal axis of the tube at about the termination of the transition region. After that, the white lines evolved to a local white area in the middle height of the specimen by fiber rowing. Finally, at the end of the linear third region, the concentrated white coloured area led to the sudden failure by fracturing of fibres.

For compacted composite concrete cylinders, failure occurred at nearly the middle of the specimen's height and progressed to its bottom and top ends with $\pm 55^{\circ}$ angle. On the other hand, for uncompacted specimens, failure initiated from top or bottom ends of specimen because of contacting GFRP tubes to the loading plate due to large deformation of concrete because of voids. This contact allowed axial load transfer to the GFRP tube directly. Therefore, local buckling causing intensive whitening and matrix failure on the contacting zone led to the final failure of the pipe (Fig. 5), combined with remarkable bulging at nearly the middle of the specimens during the mobilization of the concrete to keep the pipe from buckling. This buckling effect suddenly directed the failure to start at the top of the specimen instead of the middle region, causing a reduction of the axial load capacity.

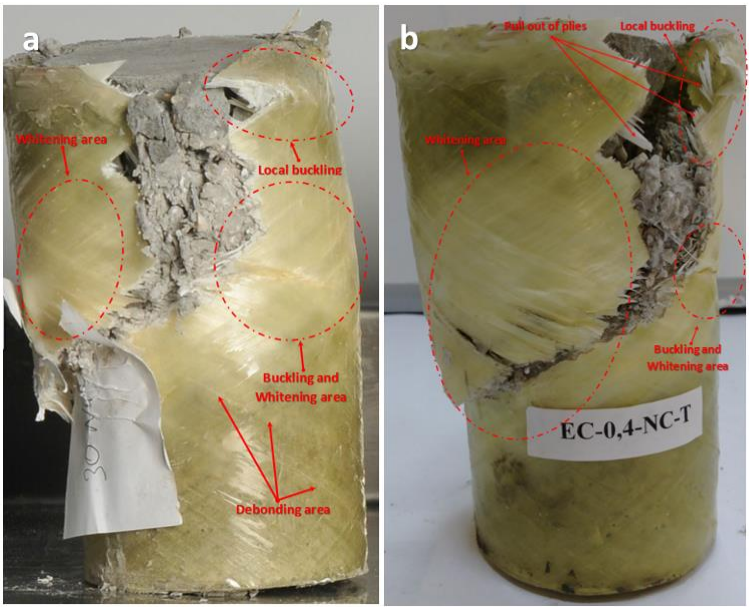

Fig. 5. Local buckling causing intensive whitening and the contacting zone led the final failure of the pipe a) specimen NC-0,5-NC-T b) specimen EC-0,4-NC-T

The axial load against displacement curves for all specimens are given in Figs. 6 to 11. It is clear from the curves that the confinement effect on concrete not only improves the axial load capacity but also increases axial deformation at failure.

The confinement effect on concrete strength and axial deformation is given in Table 4 for all confined specimens. The effect of confinement that is the difference between the axial load capacity of concrete and axial deformation at failure in confined and unconfined tubes is shown in Fig. 6. Concrete core failure in a confined specimen is assumed at the point where the axial load–deformation curve changed from linear to non-linear stage. A typical calculation of the confinement effect on PC axial displacement and compressive strength is presented in Fig. 6 for one compacted specimen with Portland cement, PC-0.4-C-T. The percentage of improvement in compressive strength of composite overwrapped concrete cylinder in comparison with unconfined concrete ones is given in Table 4. The improvement trend is higher for the concrete cylinders with the low compressive strength.

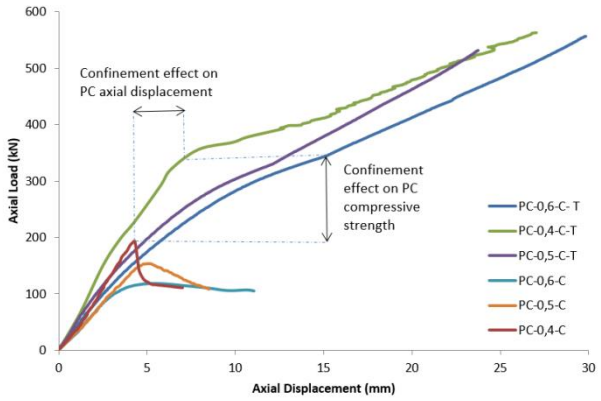

Fig. 6. Axial load-displacement curves of portland cement compacted specimens

Table 4. Properties of cylindrical specimens and results for cylindrical specimens subjected to uniaxial compression

Specimen	Cement type	Vibration used	GFRP Tube	Compressive strength at 28 days (MPa)	Max Deflection (mm)	Max Load (kN)	Ratio of confined to unconfined axial-load capacities	The confinement effect (%)	% Improvement of Compressive Strength
PC-0,6-C- T	Portland	✓	✓	17	29,67	554,12	4,76	50,00	476
PC-0,5-C-T	Portland	✓	✓	22	23,59	529,05	3,46	36,36	346
PC-0,4-C-T	Portland	✓	✓	23	26,70	559,34	2,94	39,68	294
EC-0,6-C-T	expansive	✓	✓	27	31,15	538,26	2,21	18,33	221
EC-0,5-C-T	expansive	✓	✓	32	30,72	561,59	1,93	3,33	193
EC-0,4-C-T	expansive	✓	✓	38	19,52	538,51	1,72	0,65	172
PC-0,6-NC-T	Portland	-	✓	15	32,73	456,22	4,34	52,38	434
PC-0,5-NC-T	Portland	-	✓	20	30,47	487,62	3,28	10,00	328
PC-0,4-NC-T	Portland	-	✓	22	29,63	483,62	2,72	41,38	272
EC-0,6-NC-T	expansive	-	✓	25	24,90	514,45	2,68	12,86	268
EC-0,5-NC-T	expansive	-	✓	29	23,64	527,79	2,20	20,00	220
EC-0,4-NC-T	expansive	-	✓	35	22,82	514,86	2,06	16,67	206
PC-0,6-C	Portland	✓	-	17	5,29	116,30	-	-	
PC-0,5-C	Portland	✓	-	22	4,87	152,87	-	-	
PC-0,4-C	Portland	✓	-	23	4,17	190,11	-	-	
EC-0,6-C	expansive	✓	-	27	4,39	243,74	-	-	
EC-0,5-C	expansive	✓	-	32	5,11	291,30	-	-	
EC-0,4-C	expansive	✓	-	38	5,08	312,19	-	-	
PC-0,6-NC	Portland	-	-	15	6,00	105,20	-	-	
PC-0,5-NC	Portland	-	-	20	4,76	148,67	-	-	
PC-0,4-NC	Portland	-	-	22	4,79	178,02	-	-	
EC-0,6-NC	expansive	-	-	25	3,92	192,22	-	-	
EC-0,5-NC	expansive	-	-	29	5,05	240,39	-	-	
EC-0,4-NC	expansive	-	-	35	5,49	250,03	-	-	

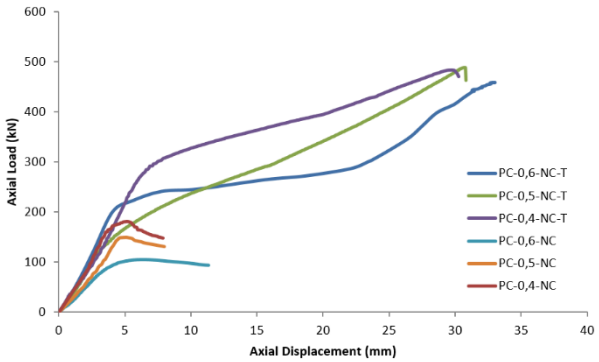

Fig. 7. Axial load-displacement curves of portland cement uncompacted specimens

Figs. 6 to 11 show that the first region of the composite tubes' axial load–deformation response coincided with that of the unconfined concrete specimens up to approximately 25%, 32%, 47% and 48% for Portland cement compacted specimens, Portland cement uncompacted specimens, expansive cement compacted specimens and expended cement uncompacted specimens, respectively.

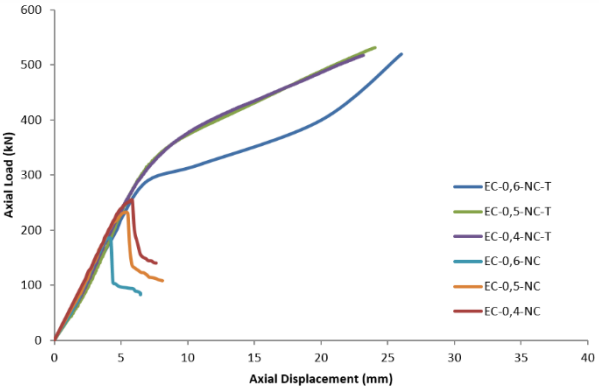

Fig. 8. Axial load-displacement curves of expansive cement uncompacted specimens

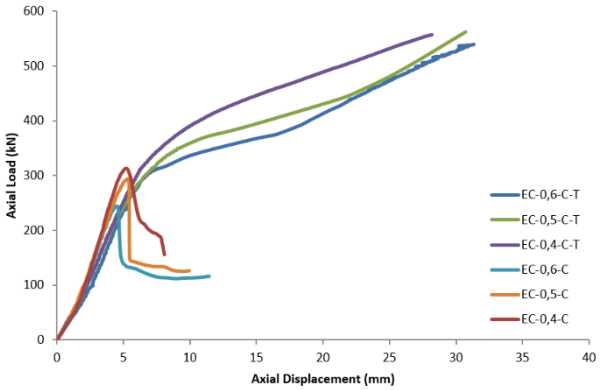

Fig. 9. Axial load-displacement curves of expansive cement compacted specimens

The ultimate axial loads of composite tubes were found to be about 3.72, 1.95, 3,44 and 2,31 times higher than those of unconfined concrete cylinders of Portland cement compacted specimens, Portland cement

uncompacted specimens, expansive cement compacted specimens and expansive cement uncompacted specimens, respectively (Table 4).

The essential difference between the behaviour of compacted and uncompacted specimens is the transition region after the first linear part of the graph. It is clearly observed from Figs. 10 and 11 that uncompacted specimens have a lower axial load capacity up to the point when the effect of confinement is mobilized. A third linear region is identified for un-compacted specimens where the effect of GFRP is dominant.

The use of expansive cement instead of Portland cement has remarkable effect on confinement effect on enhancing concrete strength and ductility under compression as observed in Figs. 10 and 11.

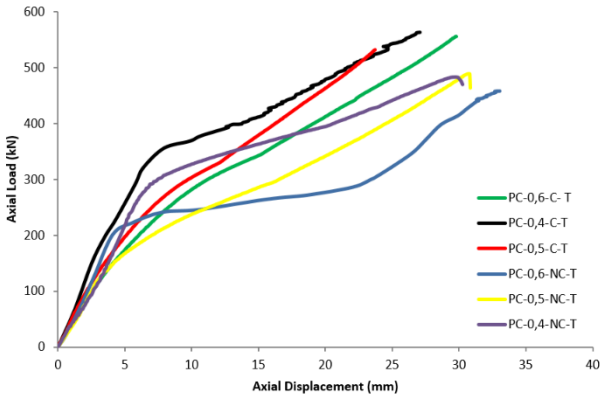

Fig. 10. Axial load-displacement curves of portland cement specimens

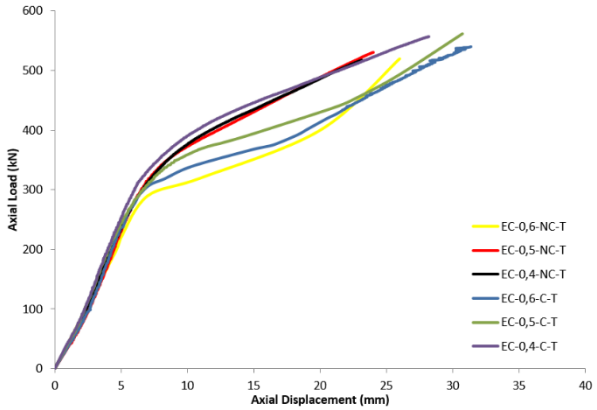

Fig. 11. Axial load-displacement curves of expansive cement specimens

3.2. Failure analysis of composite tubes and composite concrete

In this section, macro and micro analyses of failure formed on composite pipes are investigated. Macro and micro structure of 4 different specimens were studied in detail. As observed in Fig. 12, radial cross sections of failure zones for specimens EC-0.4-C-T, EC-0.4-NC-T, EC-0.6-C-T and PC-0.5-NC-T were taken and investigated under an electron microscope. The selection of these specimens is considered in order to compare the interface bonding for compacted and uncompacted specimens and to investigate the failures of specimens with different parameters, for example cement type, concrete strength represented by w/c ratio and compaction effect.

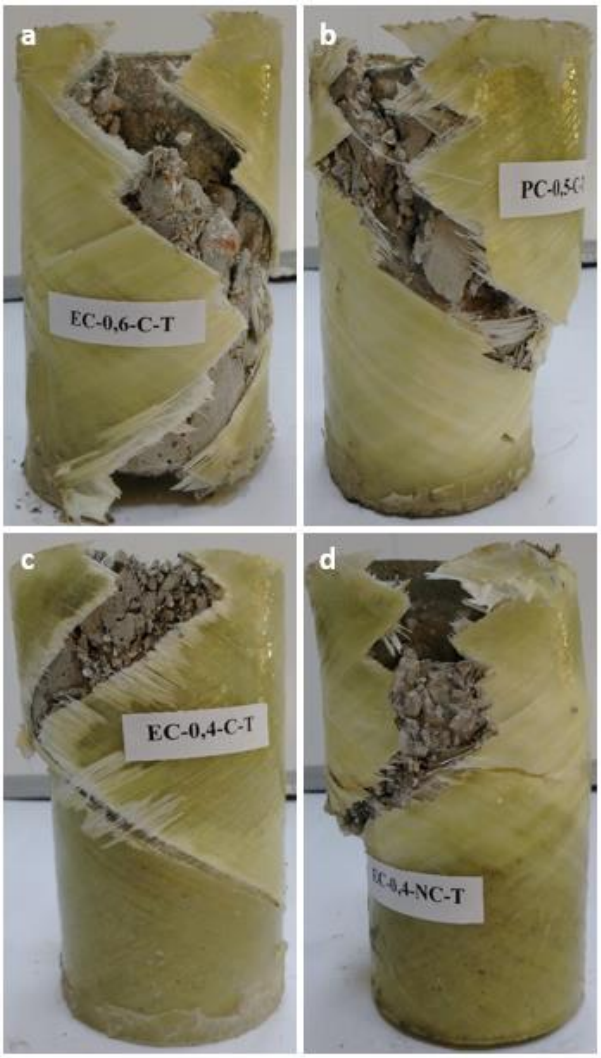

Fig. 12. Photos of final fractures of the selected specimens. a) specimen EC-0,6-C-T b) specimen PC-0,5-C-T c) specimen EC-0,4-C-T d) specimen EC-0,4-NC-T

The failure of GFRP pipe, interface between concrete core and composite pipe, the failure of concrete core and degradation of concrete were investigated under an electron microscope and presented in Fig. 13 for specimens EC-0.4 C-T and EC 0.4 NC-T.

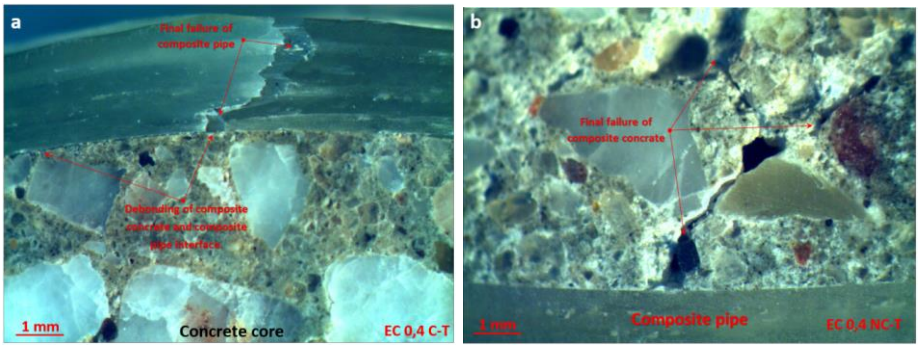

Fig. 13. a) Failure of composite pipe and interface between concrete and pipe for Specimen EC-0,4-C-T b) failure of composite concrete for Specimen EC 0.4 NC-T

Fig. 14 for specimen EC-0.4-C-T shows that, under high stress levels, the failure of concrete core occurred on both bottom and top of the cross-section, causing the formation of two truncated cones with approximately 45♂ angle on both the bottom and top of the specimens.

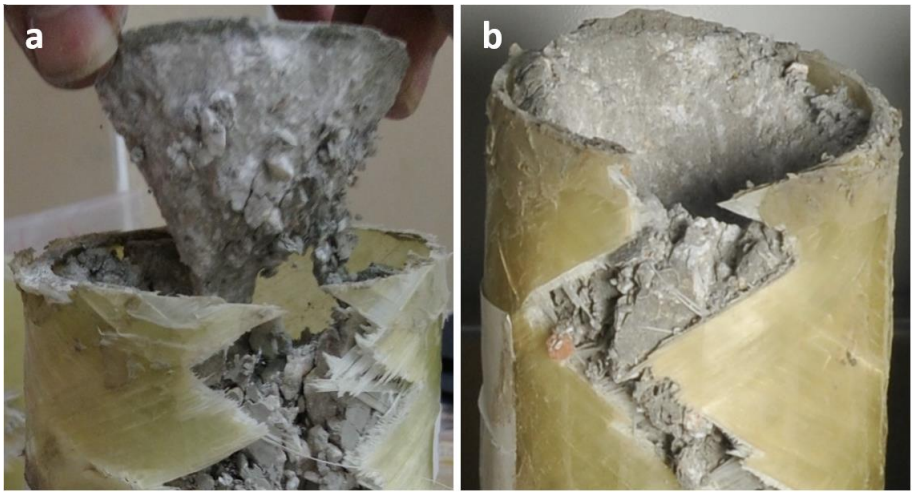

Fig. 14. Truncated pyramids with 45♂ angle on concrete core a) Top of the concrete specimen b) Bottom of the concrete specimen

Due to the confinement effect, the failure of concrete occurred at higher stress levels than unconfined concrete test specimens as the composite pipe continued to carry the increased load despite of the significant cracks in concrete. It is observed that the failure of composite tube was influenced by the progressive cracking and expansion of the concrete core, leading to composite pipe failure in the hoop direction. The damage stages of the composite pipe EC-0.4-C-T may be summarised in the four phases below.

Debonding: debonding formation at a load level of approximately 310 kN has been observed by separating the fibre matrix interface in the fibre direction due to the shape change as depicted in Fig. 5a.

Whitening: with the increase of the applied load, whitening started in the middle part of the composite pipe with the development of debonding and failure in the matrix in the range of 350 to 420 kN load level. It was observed that intense whitening occurred at around 480 kN load level (Fig. 5). Whitening on composite pipe radial section can be clearly seen in Fig. 15b.

Matrix/Transfer cracking and delamination: After whitening development, at around 400 kN load level, matrix cracking sounds began to be heard. At higher load levels between 430 kN and 500 kN, delamination failure was detected owing to the effect of radial direction deformation and shortening of the pipe on the axial direction. Fig. 15a shows the effect of delamination on the formation of layers of $(\pm 55^{\circ})_3$.

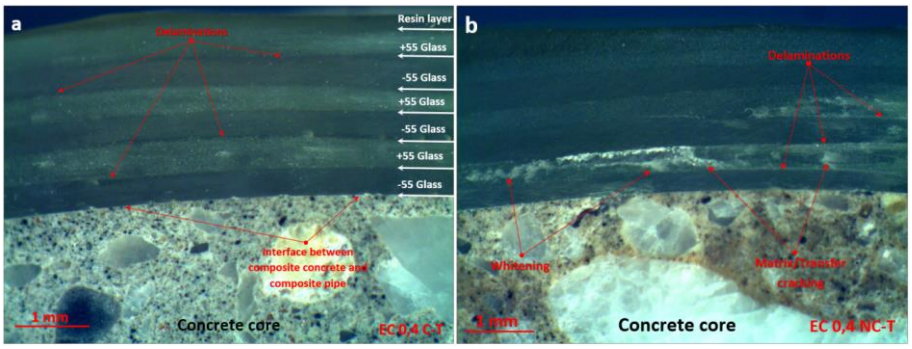

Fig. 15. a) Interface between concrete and GFRP pipe, delamination (Electron microscope photos of specimen EC-0,4-C-T) b) matrix/transfer cracking and whitening on radial sections (Electron microscope photos of specimen EC-0.4 NC-T)

Splitting: in the area where all damage is concentrated, delamination was identified (Fig. 16a). Thereafter, pin hole was observed with effect of the delamination. As observed in Fig. 16d., splitting occurs before the final failure (Fig. 16c.) that is formed by cutting the plies after delaminations, voids in the composite ply and matrix / transfer cracking (Fig. 15b) and Fig. 5a).

Final failure: Damage is mainly concentrated in the middle zone of the composite pipe where a sudden fibre break with a loud sound at a load level of 538 kN was identified. This damage started at the middle height of the specimen and advanced towards both directions axially. As seen in Fig. 12, fibre rupture is observed in the direction of winding angles with ± 55° and having a leaf-shape. When final failure occurred, whitening area is concentrated in the middle height of the specimen but, at both ends of the pipe, whitening was not observed. Final failure in the form of fibre breakages followed a zigzag line in the direction of the winding angleon (Fig. 5). After intra-ply fibre breakages were formed, inter-ply pull-out of plies failure were observed (Fig. 16b). Fig. 16 confirms that micro damage mechanisms of failure using Electron microscope including delamination, matrix/transfer cracking, splitting, fibre breakages and pull out of plies were identified.

All failures started near to the middle height of the pipes. With the increase of compression load, the failure propagated to both ends of the pipe.

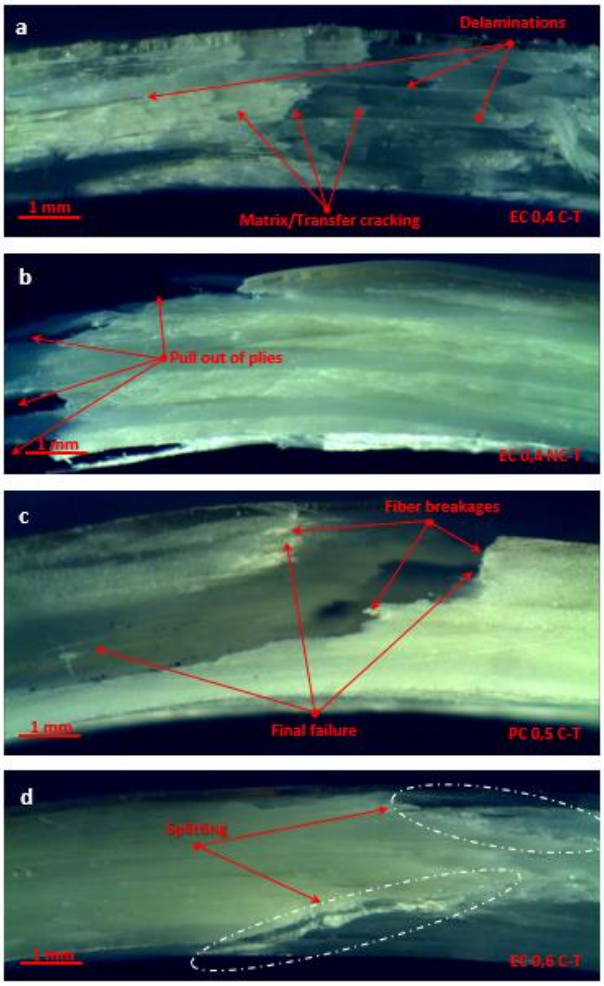

Fig. 16. Electron microscope photographs from radial sections of damaged composite pipes a) delaminations and matrix/transfer cracking b) pull out of piles c) fibre breakages d) splitting

For uncompacted concrete specimens, because of large deformation of the core concrete due to voids in concrete, the loading plate has moved to become on contact to the pipe ends. An average reduction of 20% in the axial load capacity was observed due to such voids in concrete core (Fig. 17). During the contact of loading plate and composite pipe, the pipe is crushed, accelerating the pipe failure (Fig. 5). Additionally, virgin nylon fibrous monofilament fibres in damaged composite concrete is shown in Fig. 18.

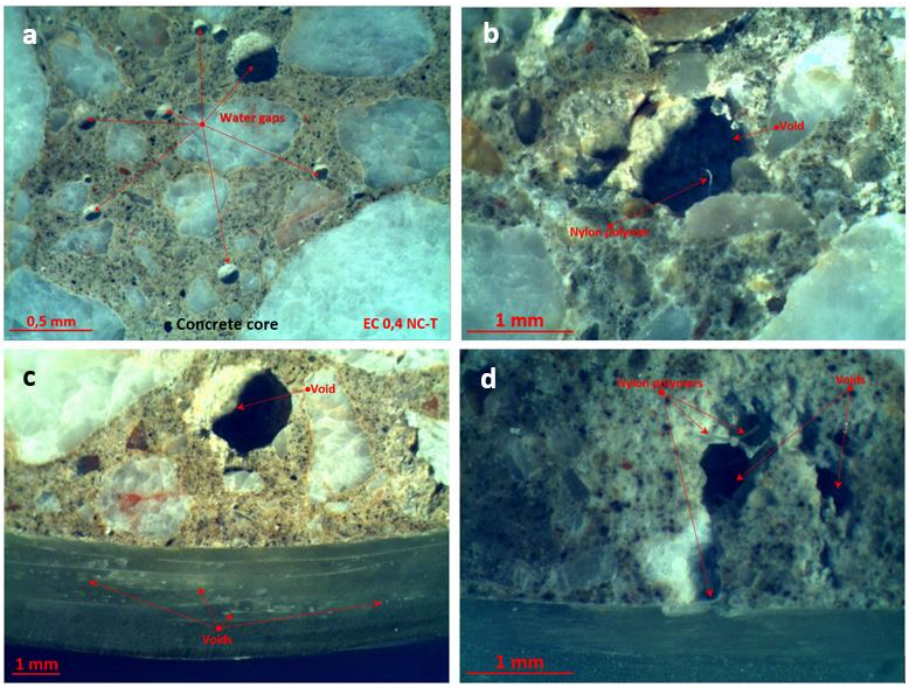

Fig. 17. Scanning electron microscope photographs uncompressed EC-0.4 NC-T specimen's cross-section a) water gaps in concrete b) void because of uncompaction c) void on pile section d) void due to accumulation of fibers

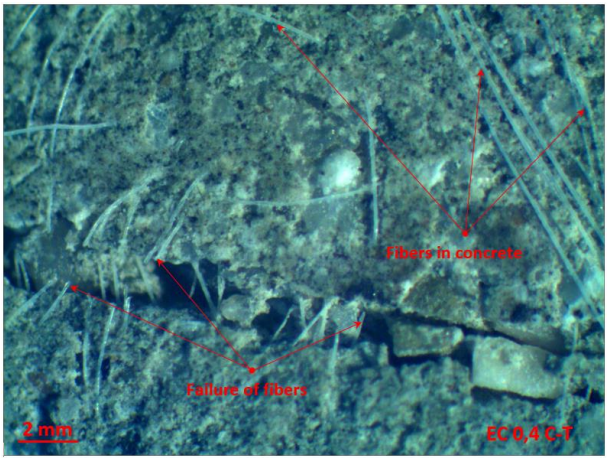

Fig. 18. Failure model of nylon polymers after failure in composite concrete in specimen EC-0.4 C –T

4. Estimation of Ultimate Compressive Strength

In a FRP confined concrete tube, lateral confinement pressure maintained by FRP wrapping to concrete is passive until the load is applied. Under axial compression loading, concrete core tends to spread out laterally. However, FRP tube restrains the concrete core to extend. Therefore, a circular tension resultant in the envelope is maintained by this expansion. The reaction occuring due to this expansion action is symbolized by a uniform lateral pressure f_l in the interface of FRP material (Fig. 19).

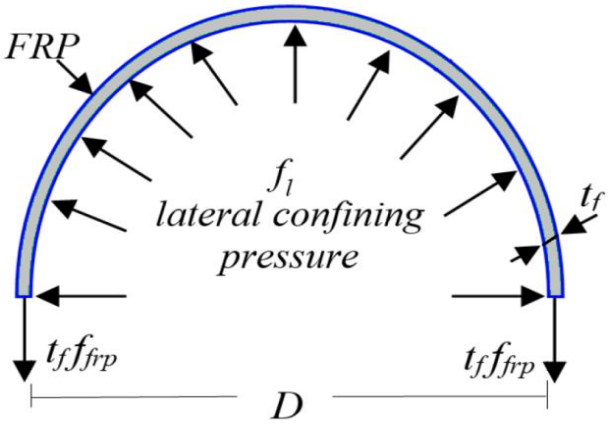

Fig. 19. Confining action of FRP shell on concrete core

From Fig. 19, considering one unit length of the pipe and using equilibrium of forces at FRP rupture, the following relation may be obtained:

$$f_l D = 2t_f f_{frp} \quad (1)$$

where f_l is the lateral confining pressure, f_{frp} is the tensile rupture strength of FRP in hoop direction, D is the concrete core diameter and t_f is the FRP thickness. Rearranging the above equation, the lateral confining pressure f_l may be written as:

$$f_l = \frac{2t_f f_{frp}}{D} = \frac{1}{2} f_{frp}\, \rho_{frp} \quad (2)$$

where ρ_{frp} is the FRP volumetric ratio, defined by:

$$\rho_{frp} = 4t_f/D \quad (3)$$

In the literature, various models for the confined compressive strength of concrete have been developed since 1968 [37-49]. Summary of these models including those recommended by various design guidelines for FRP confined concrete elements are given in Table 5.

Table 5. Summary of desing-oriented models of FRP-confined concrete

Model	Year	Strength enhancement ratio
Fardis and Khalili [39]	1982	$f_{cc} = \left(1 + 4.1\frac{f_l}{f_{co}}\right).f_{co}$
Miyauchi et al. [40]	1999	$f_{cc} = \left(1 + 2.98\frac{f_l}{f_{co}}\right).f_{co}$
Bisby et al. [41]	2005	$f_{cc} = \left(1 + 2.425\frac{f_l}{f_{co}}\right).f_{co}$
Matthys et al. [42]	2006	$f_{cc} = \left(1 + 3.5\left(\frac{f_l}{f_{co}}\right)^{0.85}\right).f_{co}$

Youssef et al. [43]	2007	$f_{cc} = \left(1 + 2.25\left(\frac{f_l}{f_{co}}\right)^{1.25}\right).f_{co}$, for ascending curves; $f_{cc} = \left(1 + 3.0\left(\frac{4E_{frp}\varepsilon_{jt}t/d}{f_{co}}\right)^{1.25}\right).f_{co}$, for descending curves
Ciupala et al. [44]	2007	$f_{cc} = \left(1 + 1.7\left(\frac{2f_l}{f_{co}}\right)^{0.8}\right).f_{co}$
Vintzileou and Panagiotidou [45]	2007	$f_{cc} = \left(1 + 2.8\frac{f_l}{f_{co}}\right).f_{co}$
Park et al. [46]	2011	$f_{cc} = \left(0.7 + 3.7\frac{f_l}{f_{co}}\right).f_{co}$
CSA (Canadian Standards Association) [47]	2002	$f_{cc} = 0.85f_{co} + 6.7{f_l}^{0.83}$
ACI (American Concrete Institute) [48]	2008	$f_{cc} = f_{co} + \left(\psi_f 3.3\frac{f_l}{f_{cc}}\right)$
TEC (Turkish Earthquake Code) [49]	2007	$f_{cc} = f_{co}\left(1 + 2.4\left(\frac{f_l}{f_{co}}\right)\right)$

Note: f_{cc} =confined concrete compressive strength; f_{co}= compressive strength of concrete core; E_{frp} = Modulus of elastisity of FRP; ϵ_{jt} = FRP jacket strain at transition from first to second region = 0.002; ψ_f= FRP strength reduction factor = 0.85 for flexure (calibrated based on design material properties) = 0.85 for shear (based on reliability analysis) for three-sided FRP U-wrap or two-sided strengthening schemes = 0.95 for shear fully wrapped sections [52]

Table 5 indicates that the unconfined concrete compressive strength and lateral confining stress by FRP wrapping are the dominant factors influcing the confined concrete compressive strength calculated by various models. Predictions of confined concrete compressive strength provided from the eleven models presented in Table 5 against the current experimental results are presented in Fig. 20.

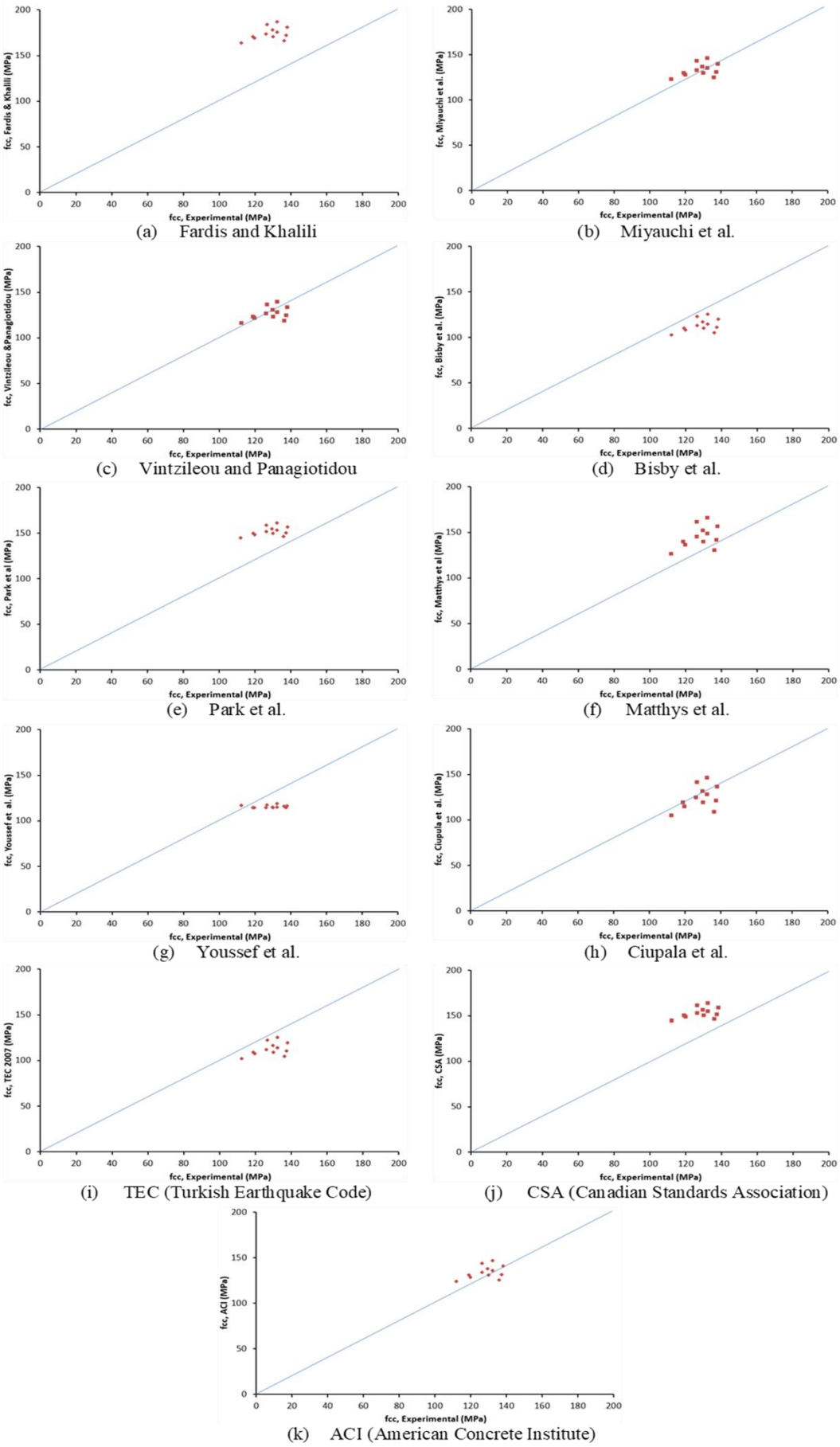

Fig. 20. Predictions of confined concrete compressive strength provided from the eleven models against the current experimental results

The confined concrete compressive strengths, f_{cc}, estimated from Fardis & Khalili 1982, Matthys et al. 2006 and CSA design guidelines, are generally higher than that obtained from experimental results. On the other hand, Bisby et al. 2005 and TEC 2007 design guidelines predicted lower confined concrete compressive strength compared with experimental results. The predictions of the design equations proposed by the ACI, Miyauchi et al. 1999, Vintzileou & Panagiotidou 2007 and Cipula et al. 2007 are quite reliable.

5. Conclusions

In this study, the behaviour of concrete-filled GFRP pipes with different compressive strengths is investigated under axial loading. Macro and micro observations of pipe failure were also studied. The experimental results were also used to assess the applicability of 11 design models available in the literature for confined concrete compressive strength. The following conclusions can be drawn:

- Concrete vibration has a clear effect on the axial load-deformation relationship, especially after the linear elastic part of loading.
- The interfacial slippage between GFRP pipes and expansive cement concrete core is relatively postponed compared with that for portland cement concrete cores, but not completely prevented.
- GFRP tube confinement of concrete cylinders increased their axial load capacity by 285% on average and their axial deformation at failure by 557% on average.
- Debonding, whitening, matrix/transfer cracking, delamination, splitting and final failure macro and micro damage mechanisms were detected within $\pm 55^{\circ}$ filament wound winding angle.
- The predictions of confined concrete compressive strength by the design guidelines of ACI, Miyauchi et al. 1999, Vintzileou & Panagiotidou 2007 and Cipula et al. 2007 are reasonably close to the experimental results. However, the predictions by other models either overestimate or underestimate the experimental results.
- The current study shows that concrete filled FRP tube cylindrical specimens offer a simple but effective to construct and steel reinforcement corrosion-free option for construction of deep pile foundations, columns, etc. However, further investigations are required to study the large-scale field implementation and performance of concrete filled FRP elements under harsh environments.

References

[1] M. Saafi, H.A. Toutanji, Z. Li, Behavior of concrete columns confined with fiber reinforced polymer tubes, ACI materials journal 96(4) (1999) 500-509.
[2] A.Z. Fam, S.H. Rizkalla, Confinement model for axially loaded concrete confined by circular fiber-reinforced polymer tubes, Structural Journal 98(4) (2001) 451-461.
[3] W.-K. Hong, H.-C. Kim, Behavior of concrete columns confined by carbon composite tubes, Canadian Journal of Civil Engineering 31(2) (2004) 178-188.
[4] T. Ozbakkaloglu, D.J. Oehlers, Manufacture and testing of a novel FRP tube confinement system, Engineering Structures 30(9) (2008) 2448-2459.
[5] T. Ozbakkaloglu, D.J. Oehlers, Concrete-filled square and rectangular FRP tubes under axial compression, Journal of Composites for Construction 12(4) (2008) 469-477.

[6] H.M. Mohamed, R. Masmoudi, Axial load capacity of concrete-filled FRP tube columns: Experimental versus theoretical predictions, Journal of composites for construction 14(2) (2010) 231-243.
[7] T. Ozbakkaloglu, Axial compressive behavior of square and rectangular high-strength concrete-filled FRP tubes, Journal of Composites for Construction 17(1) (2012) 151-161.
[8] T. Ozbakkaloglu, Compressive behavior of concrete-filled FRP tube columns: Assessment of critical column parameters, Engineering Structures 51 (2013) 188-199.
[9] T. Ozbakkaloglu, Concrete-filled FRP tubes: Manufacture and testing of new forms designed for improved performance, Journal of Composites for Construction 17(2) (2012) 280-291.
[10] T. Vincent, T. Ozbakkaloglu, Influence of concrete strength and confinement method on axial compressive behavior of FRP confined high-and ultra high-strength concrete, Composites Part B: Engineering 50 (2013) 413-428.
[11] A. Mirmiran, M. Shahawy, Behavior of concrete columns confined by fiber composites, Journal of Structural Engineering 123(5) (1997) 583-590.
[12] A. La Tegola, O. Manni, Experimental investigation on concrete confined by fiber reinforced polymer and comparison with theoretical model, Special Publication 188 (1999) 243-254.
[13] P. Rochette, P. Labossiere, Axial testing of rectangular column models confined with composites, Journal of composites for construction 4(3) (2000) 129-136.
[14] S. Pessiki, K. Harries, J. Kestner, R. Sause, J. Ricles, The axial behavior of concrete confined with fiber reinforced composite jackets, J. Compos. Constr 5(4) (2001) 237-245.
[15] G. Li, D. Maricherla, K. Singh, S.-S. Pang, M. John, Effect of fiber orientation on the structural behavior of FRP wrapped concrete cylinders, Composite structures 74(4) (2006) 475-483.
[16] G. Li, Experimental study of FRP confined concrete cylinders, Engineering structures 28(7) (2006) 1001-1008.
[17] A. Parvin, A.S. Jamwal, Effects of wrap thickness and ply configuration on composite-confined concrete cylinders, Composite structures 67(4) (2005) 437-442.
[18] A. Parvin, A.S. Jamwal, Performance of externally FRP reinforced columns for changes in angle and thickness of the wrap and concrete strength, Composite Structures 73(4) (2006) 451-457.
[19] T. Vincent, T. Ozbakkaloglu, Influence of fiber orientation and specimen end condition on axial compressive behavior of FRP-confined concrete, Construction and Building materials 47 (2013) 814-826.
[20] N. Tarakçioğlu, L. Gemi, A. Yapici, Fatigue failure behavior of glass/epoxy±55 filament wound pipes under internal pressure, Composites Science and Technology 65(3) (2005) 703-708.
[21] I.F. Kara, A.F. Ashour, M.A. Köroğlu, Flexural behavior of hybrid FRP/steel reinforced concrete beams, Composite Structures 129 (2015) 111-121.
[22] I.F. Kara, A.F. Ashour, M.A. Köroğlu, Flexural performance of reinforced concrete beams strengthened with prestressed near-surface-mounted FRP reinforcements, Composites Part B: Engineering 91 (2016) 371-383.
[23] I.F. Kara, M.A. Köroğlu, A.F. Ashour, Tests of continuous concrete slabs reinforced with basalt fibre reinforced plastic bars, ACI Structural Journal (2017) 114(5) 1201-1213.
[24] L. Gemi, N. Tarakçioğlu, A. Akdemir, Ö.S. Şahin, Progressive fatigue failure behavior of glass/epoxy (±75) 2 filament-wound pipes under pure internal pressure, Materials & Design 30(10) (2009) 4293-4298.
[25] R. Rafiee, F. Elasmi, Theoretical modeling of fatigue phenomenon in composite pipes, Composite Structures 161 (2017) 256-263.
[26] A. Hawa, A. Majid, M. Afendi, M. Haslan, K. Pranesh, N. Amin, Burst strength of glass fibre/epoxy composite pipes subjected to impact loading, Applied Mechanics and Materials, Trans Tech Publ, 2015, pp. 121-125.
[27] Ö.S. Sahin, A. Akdemir, A. Avci, L. Gemi, Fatigue crack growth behavior of filament wound composite pipes in corrosive environment, Journal of Reinforced Plastics and Composites 28(24) (2009) 2957-2970.

[28] L. Gemi, M. Kara, A. Avci, Low velocity impact response of prestressed functionally graded hybrid pipes, Composites Part B: Engineering 106 (2016) 154-163.
[29] R. Rafiee, B. Mazhari, Simulation of the long-term hydrostatic tests on Glass Fiber Reinforced Plastic pipes, Composite Structures 136(Supplement C) (2016) 56-63.
[30] R. Rafiee, F. Reshadi, Simulation of functional failure in GRP mortar pipes, Composite Structures 113(Supplement C) (2014) 155-163.
[31] A. Castellano, P. Foti, A. Fraddosio, S. Marzano, M.D. Piccioni, Mechanical characterization of CFRP composites by ultrasonic immersion tests: Experimental and numerical approaches, Composites Part B: Engineering 66 (2014) 299-310.
[32] L. Gemi, Ö.S. Şahin, A. Akdemir, Experimental investigation of fatigue damage formation of hybrid pipes subjected to impact loading under internal pre-stress, Composites Part B: Engineering 119 (2017) 196-205.
[33] A. Standard, D1599, 1999 (2005)," Standard Test Method for Resistance to Short-Time Hydraulic Pressure of Plastic Pipe, Tubing, and Fittings," ASTM International, West Conshohocken, PA, 2006, DOI: 10.1520/D1599-99R05.
[34] T. EN, 206-1. 2002, Beton-Bölüm 1: Özellik, Performans, İmalat ve Uygunluk (2002).
[35] M. Touhari, R. Mitiche-Kettab, Behaviour of FRP Confined Concrete Cylinders: Experimental Investigation and Strength Model, Periodica Polytechnica. Civil Engineering 60(4) (2016) 647.
[36] T. Xie, T. Ozbakkaloglu, Behavior of steel fiber-reinforced high-strength concrete-filled FRP tube columns under axial compression, Engineering Structures 90 (2015) 158-171.
[37] S. Guler, A. Ashour, Review of Current Design Guidelines for Circular FRP-Wrapped Plain Concrete Cylinders, Journal of Composites for Construction 20 (2016) article number 04015057.
[38] L. Huang, C. Gao, L. Yan, B. Kasal, G. Ma, Reliability assessment of confinement models of carbon fiber reinforced polymer-confined concrete, Journal of Reinforced Plastics and Composites 35(12) (2016) 996-1026.
[39] M.N. Fardis, H.H. Khalili, FRP-encased concrete as a structural material, Magazine of concrete research 34(121) (1982) 191-202.
[40] K. Miyauchi, S. Inoue, T. Kuroda, A. Kobayashi, Strengthening effects with carbon fiber sheet for concrete column, Proc Jpn Concr Inst 21(3) (1999) 1453-1458.
[41] L.A. Bisby, A.J. Dent, M.F. Green, Comparison of confinement models for fiber-reinforced polymer-wrapped concrete, ACI Structural Journal 102(1) (2005) 62.
[42] S. Matthys, H. Toutanji, K. Audenaert, L. Taerwe, Axial load behavior of large-scale columns confined with fiber-reinforced polymer composites, ACI Structural Journal 102(2) (2005) 258.
[43] M.N. Youssef, M.Q. Feng, A.S. Mosallam, Stress–strain model for concrete confined by FRP composites, Composites Part B: Engineering 38(5) (2007) 614-628.
[44] M. Ciupala, K. Pilakoutas, A. Mortazavi, Effectiveness of FRP composites in confined concrete, Proceedings of the 8th international symposium on fiber reinforced polymer reinforcement for concrete structures, University of Patras, Patras, Greece, 2007.
[45] E. Vintzileou, E. Panagiotidou, An empirical model for predicting the mechanical properties of FRP-confined concrete, Construction and Building Materials 22(5) (2008) 841-854.
[46] J.-H. Park, B.-W. Jo, S.-J. Yoon, S.-K. Park, Experimental investigation on the structural behavior of concrete filled FRP tubes with/without steel re-bar, KSCE Journal of Civil Engineering 15(2) (2011) 337-345.
[47] C.S. Association, Design and construction of building components with fibre-reinforced polymers, Canadian Standards Association2002.
[48] C.E. Bakis, A. Ganjehlou, D.I. Kachlakev, M. Schupack, P. Balaguru, D.J. Gee, V.M. Karbhari, D.W. Scott, C.A. Ballinger, T.R. Gentry, Guide for the design and construction of externally bonded FRP systems for strengthening concrete structures, Reported by ACI Committee 440(2002) (2002).
[49] T.S. Code, Ministry of public works and settlement, Specification for Structures to be Built in Disaster Areas, Government of Republic of Turkey (2007).